O_2-assisted Water Gas Shift reaction over structured Au and Pt catalysts

M. González-Castaño[*], T. R. Reina[1], S. Ivanova, L. M. Martínez Tejada, M. A. Centeno, J. A. Odriozola.*

Departamento de Química Inorgánica e Instituto de Ciencia de Materiales de Sevilla (ICMS), Centro mixto CSIC-Universidad de Sevilla, Avda. Americo Vespucio 49, 41092 Sevilla, Spain

corresponding author: *miriam.gonzalez@icmse.csic.es ; t.ramirez-reina@imperial.ac.uk*

Abstract: Platinum and gold structured catalysts were compared as active phases in classical and O_2-assisted Water Gas Shift (WGS) reaction. Both metals were supported on iron-doped ceria mixed oxide and then, structured on metallic micromonolithic devices. As expected the WGS activity of both micromonoliths is conditioned by the nature of the noble metals being Pt the most active metal in traditional conditions. However, the addition of oxygen to the classical water gas feed turns the balance in favor of the gold based catalysts, being the presence of gold responsible for an excessive improvement of the catalytic activity.

Keywords: *Water Gas Shift, O_2-assisted Water Gas Shift, micromonolith, platinum, gold, ceria.*

[1]Actual corresponding author address: Department of Chemical Engineering, Imperial College London, London SW7 2AZ. t.ramirez-reina@imeperial.ac.uk

1. Introduction

Among the new energy sources, hydrogen is recognized as the most promising future fuel because it is a clean, renewable and highly efficient energy carrier. The chemical energy of H_2 can be converted into electricity by using fuel cells with great energy efficiency. Nevertheless the overall process of feeding a fuel cell with hydrogen involves a series of processing steps of production and especially orientated to purify the H_2 stream by removing the unavoidably generated CO traces in the reforming reaction [1]. Among these processing stages the Water Gas Shift (WGS, $CO + H_2O \leftrightarrow CO_2 + H_2$) represents the most important process. The WGS is an exothermic reaction favored with the temperature but also thermodynamically limited. Moreover, it requires elevated contact times to obtain acceptable CO conversion levels, which in turn results in relatively high reactor volumes. This fact represents a drawback especially when mobile applications are targeted. Therefore, the success of H_2 technology for portable devices heavily depends on minimizing the WGS unit volume.

The use of structured reactors represents an interesting approach in order to face the residence time issues [2]. In particular, micromonolithic structures are interesting devices that allow a noteworthy reactor volume decrease and facilitate the incorporation of the WGS unit for mobile applications [3,4]. Moreover, the low pressure drop and high mechanical strength consented by the use of micromonoliths appear as an optimal alternative to powder fixed beds. Within the types of micromonoliths in comparison to the generally used, ceramic honeycomb monoliths, their metallic homologues present higher

thermal conductivities, greater geometric surface area per volume and easier manufacture. The uniformity of the catalytic layer is assured by the washcoating method [5–7].

Although the advantages provided by the structured reactor devices are desirable for a presumable on board H_2 production, the development of highly active WGS catalysts is mandatory [8–10]. Noble metal (NM) based catalysts have been proposed as excellent candidates especially when supported on cerium oxide [11–13]. In comparison with other non-reducible supports, the benefits of using ceria based materials is commonly attributed to the Ce^{4+}/Ce^{3+} inter-conversion capacity, oxygen exchange and participation in the reaction mechanism [14–17]. In other words, ceria based supports are not mere spectators becoming a key choice feature for attaining well-designed WGS catalysts. Additionally, ceria could undergo easily support modifications directed to enhance the above mentioned redox properties. A very useful strategy is for example the use of aliovalent dopants such as Fe^{3+}, Eu^{3+} [18-22].

Going back to the NM, gold and platinum have been reported as active metals with desirable characteristics [12,18–22]. Gold based catalysts exhibit a lower operational temperature window than platinum while the latter is able to keep higher CO conversions in H_2 and CO_2 presence [12], variations usually correlated with the platinum ability to activate water [23,24]. This implies that platinum is able to perform the WGS by itself meanwhile gold needs support assistance for the water dissociation step [25–27].

Along with the catalytic activity, the deactivation effects should be considered. More precisely, the over-reduction of ceria and the formation of carbonaceous species blocking the catalysts' active sites are the most frequent phenomena leading to activity depletion

[28–33]. Although these catalytic performances can be almost fully recovered by O_2/air treatment, a stop in the process to perform such a thermal procedure is not suitable during continuous operational conditions [28,34,35]. Therefore, in order to mitigate the deactivation effects, small oxygen amounts can be directly added to the feed stream: the as called O_2-assisted WGS [35,36] with the presumption to extend the catalytic system life-time. In the literature, most of the studies related to O_2-assisted WGS concerns bimetallic Cu-based catalysts. Indeed, some promising results were published by Kughai et *al.* [35] for bimetallic Pt-Cu/CeO_2 catalysts. The remarkable enhancement of the H_2 yields with the addition of oxygen was attributed to oxygen improved CO oxidation on the metal surface leading to higher concentrations of exposed metallic active sites and, thus, to enhanced catalytic activity. The O_2-assisted WGS reaction over Au/ceria and AuCu/ceria based catalysts was also study by Gamboa-Rosales et *al.* [34] affirming that the water dissociation should be favored by the O_2 presence. Flytzani-Stephanopoulos group's presented a comparison using powder Au and Pt catalysts for the O_2 assisted WGS concluding that small amounts of gaseous oxygen (air) added to the feed gas stabilizes nano-structured Au-ceria and Pt-ceria catalysts for the shift reaction in H_2-rich gases and start/stop operation [19]. To the best of our knowledge, no studies devoted to the O_2 assisted WGS reaction using structured catalysts are published in the literature, which leads to the main aim of this work.

This paper is focused on the application of platinum and gold based structured catalysts in the WGS reaction aiming to overcome the reactor volume restrictions associated to the shift process in conventional packed bed reactors and taking advantage of the excellent mass and heat transfer properties provided by the structured systems. The effect of the structuration

process in the powder catalysts is also a subject of this study. Moreover, the influence of the oxygen on the catalytic performance of both systems is analyzed and correlated to the metal nature, catalyst state and/or reaction conditions.

2. Experimental

2.1. Monolithic manufacture

The metallic micromonoliths were prepared by rolling a flat and corrugate metal sheets, ferritic stainless steel (Fecralloy), in order to produce cylindrically shaped body composed by parallel and longitudinal flow gas channels. Geometrically, the micromonolithic structures are cylinders of 3 cm height, 1.6 cm external diameter resulting in 540 cm^2 surface area and cell density of 2067 cpsi. Before coating the micromonoliths were thermally pretreated at 900^{o}C/22h in order to grow a α-Al_2O_3 surface layer required for better catalyst anchoring [37–39].

2.2. *Support and catalysts synthesis*

Ceria-iron mixed oxide supported on high surface γ-Al_2O_3 (Sasol) was selected as support. The targeted amount of ceria iron mixed oxide on alumina was fixed to 20 wt. % and deposited by impregnation of desired amounts of $Ce(NO_3)\cdot 6H_2O$ and $Fe(NO_3)\cdot 9H_2O$ (Aldrich). The impregnation was performed in 50 mL of ethanol, evaporated in rotavapor. The achieved solid was treated with a 10M NH_4OH solution during 30 min with the purpose to assure the conversion of the initial nitrates to hydroxides. Then, the support was filtered, dried and calcined at 450 ºC during 4h using 10 ºC/min heating ramp. The nominal composition of the iron-doped ceria mixed oxide expressed in molar composition was $Ce_{0.8}Fe_{0.2}O_{2-x}$.

Gold was deposited by using $HAuCl_4$ (Alfa Aesar) as precursor and direct anionic exchange method assisted by ammonia as a method of preparation [40] being 2 wt.% the nominal gold content. The catalyst precursor was then calcined at 350 ºC for 4h with 10 ºC/min heating ramp.

On the other hand, 2 wt.% of platinum were deposited by wetness impregnation using aqueous solution of $[Pt(NH_3)_4](NO_3)_2$ (Johnson Matthey) precursor at reduced pressure in rotatory evaporator at 80 ºC. The obtained solid was calcined at 350ºC during 8h with 5ºC/min heating ramp.

From the chosen nomenclature the oxygen and the molar proportions of the components were omitted for briefness, e.g. for the support $Ce_{0.8}Fe_{0.2}O_2/Al_2O_3$ the CeFeAl is used and for the $Pt/Ce_{0.8}Fe_{0.2}O_2/Al_2O_3$ and $Au/Ce_{0.8}Fe_{0.2}O_2/Al_2O_3$ catalysts Pt/CeFeAl and Au/CeFeAl, respectively.

2.3. Washcoating method

For the slurry preparation, the catalysts were milled and the fraction inferior to 10μm retained. The rheological properties were properly adjusted in order to ensure homogeneous layer deposition and to avoid cracking effects of the layer during drying and calcination. Polyvinyl alcohol (PVA) was added as tensioactive agent to facilitate the capillary ascension of the suspension within the channels. The suspension stability was maintained by surfactant addition, e.g. colloidal γ-Al_2O_3, 20 wt.% (Nyacol). The coating procedure consists in the immersion of the monolith in the colloidal suspension for 1 min and subsequently withdrawn at constant speed of 3 cm/min. To avoid obstruction of the monoliths channels, the excess of colloid was removed by centrifugation at 700 rpm for 10

min. The deposition process is repeated till 1 g of catalyst was coated. Finally, the micromonoliths were dried at 120 ºC and calcined at the temperature corresponding of the catalyst treatment (350 ºC) at 2 ºC/min heating rate. In order to determine if any important modifications were achieved on the powder catalysts during the suspension preparation, the later was dried and calcined for using in the catalytic tests.

The adherence of the catalyst layer to the metallic substrate was analyzed by immersing the monolith in acetone during 30 min in ultrasonic bath. Once dried, the adherence was estimated from the mass lost during the treatment.

Then in the selected nomenclature M_ was standing for micromonoliths and S_ for the powder obtained from the calcined suspension; M_Pt/CeFeAl and M_Au/CeFeAl for the monoliths and S_Pt/CeFeAl and S_Au/CeFeAl for the corresponding powders resulting from the slurries used.

Characterization techniques and catalytic activity measurements

The chemical composition of the samples was measured by X-Ray fluorescence (XRF) spectrometry carried out in an X Panalytical AXIOS PW4400 using Rh tube as X-ray source. Textural properties were analyzed by N_2 adsorption-desorption measurements at liquid nitrogen temperature. The experiments were carried out on a Tristar II instrument and before the measurement, the systems were degassed at 150 ºC in vacuum during 2h. The instrument used for the X-ray diffraction (XRD) analysis was the X`Pert Pro PANalytical using Cu Kα radiation (40 mA, 45kV). The experiments were performed in 2Θ-range of 10 to 95º with position-sensitive detector using a step size of 0.05º and a step

time of 240 s. Scanning electron microscopy (SEM) study was performed in a JEOL 5400 microscope of a small part of the monolith device.

H_2-TPR experiments were carried out using 50 mg of sample charged in a conventional U-shaped reactor as a function of temperature with constant heating rate of 10 $^oC \cdot min^{-1}$ till 900 ^oC. 50 $mL \cdot min^{-1}$ certified 5% H_2 in Ar gas mixture was used and the H_2 consumption was followed by TCD detector and quantified by using CuO standard (99,999%). A molecular sieve 13× was used to retain the H_2O produced during the reduction and/or CO_2 which could be desorbed from the solid surface.

The catalytic activity was tested using a tubular fixed bed reactor at atmospheric pressure. The powder bed volume was $1.5cm^3$ and all the solids were sieved between $600 < \phi < 800\mu m$. While the gold based catalysts were not activated prior the reaction, the platinum based ones were pre-reduced in 10 vol.%H_2 /N_2 stream at 350 ^oC during 2h. The GHSV was maintained constant at 4000 h^{-1}. The classical WGS mixture was composed by 4.5vol.% CO and 30 % H_2O balanced in N_2 while the O_2-assisted WGS was carried out with a feed constituted by 0.7 vol.% O_2 + 4.5% CO + 30% H_2O balanced in N_2. For the CO oxidation test, the feed composition excluded water from the stream (0.7% O_2 + 4.5% CO in N_2). The reaction products and reactants (CO, CO_2 and H_2O) were analyzed by on-line ABB gas analyzer which is equipped with an IR detector and the activity was expressed in terms of CO conversion.

3. Results and discussion

The chemical compositions of the prepared solids are presented on Table 1. All the obtained catalyst show compositions very closed to the targeted ones. However some

changes are detected between the catalysts and the employed suspensions, such as noble metal content decrease and alumina loadings increment, variations attributed to the addition of colloidal alumina during the slurries preparation.

The textural properties of the synthesized materials are listed in Table 1. Although a specific surface area diminution was observed for all solids respect to the initial γ-Al_2O_3, rather high specific surface area systems are achieved. Minor increase of the specific surface area is observed with the addition of both NM to the CeFeAl support. Even so, all the solids show similar texture features ruled by the primary γ-Al_2O_3 matrix. On the other hand platinum incorporation does not lead to any change on the V_{pore} values; meanwhile the gold deposition slightly increases them. For gold based catalysts, this increase was previously observed and ascribed to the gold particles placement inside the support pores [41].

The suspension preparation leads to higher surface areas and V_{pore} values compared to the corresponding catalyst, due to the textural properties of the colloidal alumina (192 m^2/g; 0.58cm^3/g) used for the slurry synthesis. The obtained textural values are in good agreement with the theoretical ones received by calculation supposing a physical mixture of both, catalyst and colloidal alumina.

Figure 1 presents the XRD patterns obtained for the support, catalysts and slurries. The CeFeAl support exhibits the typical diffractions pertaining to the γ-Al_2O_3 (JCDPS# 00-48-0267) and CeO_2 (JCDPS# 00-004-0593) phases, whereas no diffraction lines for iron species are discerned. In turn, the main ceria diffraction (111) appears slightly shifted to higher 2Θ values with respect to pure ceria ones. The lattice parameter for CeFeAl system

was estimated from the (111) ceria diffraction (where minor contribution of γ-Al_2O_3 phase is detected) by using the $d = \sqrt{\frac{a}{(k^2+l^2+m^2)}}$ equation, typical for a cubic cell. Lattice parameter decrease is noticed with respect to a pure ceria lattice (5.39Å for CeFeAl *vs.* 5.40 Å for CeAl). Considering that the ionic radii of the Ce^{4+} and Fe^{3+} are respectively 0.97 and 0.64 Å, substitutional Ce-Fe solid solution formation could explain the lattice contraction and the shift of the ceria reflections towards higher 2 theta angles.

As for the catalysts, no diffraction lines for platinum neither for gold are detected, indicating that the NM phases are well dispersed on the support with presumably lower particle sizes than the detection limit, typically around 4nm.

XRD patterns of the prepared slurries resemble those of the catalysts indicating that this procedure does not entail any important change on the catalysts' structures. A new Al_2O_3 (JCDPS# 01-083-2384) phase can be discerned for the calcined slurries being the latter attributed to the boehmite phase present in the colloidal alumina solution employed as suspension stabilizer during the micromonolith preparation.

Regarding all structured catalysts, the adherence test results at around 96% of catalyst weight preservation after the test. The homogeneity of the catalytic layer was confirmed by SEM imaging. A selected microphotograph of the M_Au/CeFeAl structured catalyst is shown in Figure 2a in front section and on Figure 2b, in a cross section imaging. The α-Al_2O_3 layer generated during the pretreatment of the bare Fecralloy monolith has a needle-like structure [37] and acts as ideal surface to anchor and disperse the catalyst. As shown in the figures, the catalytic layer is perfectly settled on this oxide film with assured homogeneity by the alumina layer. The estimated theoretical layer thickness of around 8,6

μm appears to be in a good concordance with the layer thickness observed by SEM (7,5-10 μm). Assuming a perfect and homogeneous coating the theoretical layer thickness was obtained from the estimation of the volume of the coating. For this purpose, the total area of the microchannels (60 cm^2), the mass of the coverage (1000 mg), the pores volume of the dried slurry (0.41 cm^3/g) and the apparent density of the deposited solid (5.9 g/cm^3) were considered as recently reported elsewhere [42]. From the layer thickness estimation, the average particle size could be calculated by supposing spherical particles deposited onto the micromonolithic devices using the following equation: $L = d_p/6$ where L is the layer thickness and d_p is the particle diameter [43]. In our case the particles deposited into micromonoliths, present an average particle size around 52 μm.

Hydrogen temperature programmed reduction studies (H_2-TPR) were conducted in order to study the redox properties of the noble metal based catalysts and to analyse the interaction between the different metallic species and the support. Figure 3 shows the TPR profile of the studied systems. For the CeO_2-FeO_x/Al_2O_3 mixed support two reduction zones can be clearly seen in the temperature range (300–600°C). According to the samples chemical composition most of reduction should come from ceria, but iron oxide reduction is also plausible. Typically, ceria surface reduction takes place at around 400-600 ^{0}C [44] while iron oxide can be sequentially reduced as follows: $Fe_2O_3 \rightarrow Fe_3O_4$ at about 400 °C, $Fe_3O_4 \rightarrow$ FeO at about 600°C and finally FeO → Fe at higher temperatures [45]. However for iron-doped ceria these temperatures maybe shifted and the processes may overlap due to the intimate Ce-Fe interaction. In fact the two reduction peaks observed for the support likely involve both iron oxide and cerium oxide reduction processes that are not possible to split.

The addition of the noble metals alters the TPR profiles. The presence of gold or platinum decreases the temperature of reduction by facilitating the mobility of the H_2 molecule on the surface of the solid. Also some new reduction processes appear. For instance regarding the gold based system, the addition of gold provoked the apparition of three peaks instead of the two original ones. The low temperature reduction zone (centred at 150°C) is assigned to the noble metal promoted ceria surface reduction while the medium temperature process (300-500 ^{0}C) and the high temperature one (600-800 ^{0}C) could be associated to ceria and iron simultaneous reduction as reported elsewhere [46]. The last zone (600-800 ^{0}C) probably involves bulk ceria reduction also [44].

Regarding the PtCeFeAl catalyst, four different H_2 consumption processes were observed as a function of the temperature. At low temperatures (90-220 ^{0}C) a peak with a shoulder appears accounting for the simultaneous reduction of platinum and ceria surface species. Pt incorporation favours ceria reducibility as evidenced by the significant decrease of the support reduction temperature which also points out a strong Pt-support interaction [47]. This low temperature reduction zone differs from that observed in the AuCeFe catalyst. Apparently, ceria surface reduction starts sooner in the presence of Pt than in the presence of Au. In other words, Pt seems to enhance in a larger extension the support reducibility, especially in the relevant temperature range for the WGS. The second reduction zone presents two processes with different intensity ranging from 300 to 700 ^{0}C that may account for the reduction of ceria particles with either bigger particles size or poorer Pt-CeO_2 interaction. Also certain contribution of iron species reduction may happen in this temperature range as commented above. Finally in the high temperature range, ceria bulk reduction takes places at temperatures above 850 ^{0}C.

The catalytic WGS activity of both powder catalysts, Pt/CeFeAl and Au/CeFeAl, is presented in Figure 4. Both catalysts reach the equilibrium CO conversion but in a different temperature windows. While the Pt/CeFeAl arrives to a full conversion regime at 230 ºC the Au/CeFeAl catalyst shows similar results 100 ºC later. The higher activity of Pt could be related among other effects (such as the noble metal nature) to the different reducibility shown by both catalysts. As demonstrated in the TPR experiments, PtCeFeAl sample has greater reducibility and therefore higher oxygen mobility at low temperatures, a key point to achieve good WGS performance [3]. Moreover, a different activity profiles for both catalysts are detected indicating dissimilar kinetics and/or reaction pathways within the classical WGS reaction. Concerning the S_Pt/CeFeAl and S_Au/CeFeAl samples (Figure 4), both systems show lower CO conversions in comparison to their parent catalysts possibly due to the slightly lower NM content of the slurries. However, this activity decrease is less evident for the platinum based catalyst. The S_Au/CeFeAl sample, exhibits significant CO conversions yield diminutions when compared to the initial Au/CeFeAl sample. It appears that the activity of the gold based catalyst is much more influenced by the washcoating process. Different reasons could be suggested such as partial covering of the active sites by the colloidal alumina, gold sintering because of the second calcination procedure or even lower specific reaction rate of the resulting slurry.

The catalytic activity of the structured catalysts, M_Pt/CeFeAl and M_Au/CeFeAl at equal reaction mixture and GHSV= 4000 h^{-1} is presented in Figure 5a. All structured catalysts are considerably less effective in the WGS reaction respect to their parent powder samples, being uniquely the M_Pt/CeFeAl able to reach the equilibrium conversion at high temperatures (340 °C). In comparison to the fixed powder bed catalysts, the observed

activity decrease for structured catalysts could be related to the different particle sizes employed during the catalytic test, 600-800 μm for the powder catalysts and estimated 52 μm for the catalytic layer of the micromonoliths and the different rate of diffusion for the samples. Even at these conditions, the M_Pt/CeFeAl sample exhibits superior catalytic performance than its homologous M_Au/CeFeAl, reaching a maximum CO conversion of 31%.

Very interestingly, the inclusion of small amounts of oxygen in the WGS stream completely changes the picture. For the O_2-assisted WGS reaction (Figure 5a), the M_Au/CeFeAl catalyst becomes remarkably more active than M_Pt/CeFeAl one, especially in the low temperature range. Despite oxygen addition affects positively both Au and Pt based systems, the activity boosting effect is dramatically greater when gold is used as active metal. This observation is particularly interesting in view of the poor activity reached by this material in the conventional WGS test.

Given the well-known activity of the gold nanoparticles for total CO oxidation, it could be argued that the observed promotional effect is a mere coupling issue of WGS and CO oxidation reactions acting together to abate CO. In order to obtain conclusive results, the direct CO oxidation reaction ($CO + \frac{1}{2}O_2 \rightarrow CO_2$) was separately performed for both structured catalysts and the results are presented on the Figure 5b. Both structured catalysts show in the whole temperature range, the maximal CO conversion, being the later stoichiometrically limited to 31 % by the O_2 amount (0.7 vol.%) in the feed.

When analyzing in details the CO conversion in the O_2 assisted WGS reaction, it should be underlined that the 31% of conversion obtained in CO oxidation is exactly the same

conversion enhancement observed for the M_Pt/CeFeAl. In agreement with Duprez et al. [36], this improvement of the catalytic activity appears to be uniquely due to an additive effect of both, WGS and total CO oxidation reactions. Therefore, in the case of Pt the beneficial effect of oxygen is not exactly an O_2-assisted WGS but rather the result of two parallel reactions consuming CO. Moreover the difference between CO conversion in O_2-WGS and classical WGS is attenuated when temperature increases pointing to the preference of the M_Pt/CeFeAl catalyst to react via WGS instead through CO oxidation route. In fact, once the adsorbed CO (on the noble metal and/or on support surface) reacts via CO oxidation and the products of the reaction are evacuated, the concentration of the available active sites to react via WGS reaction (slower reaction) should increase and the WGS should become preferred at higher temperature where the rate of evacuation of the products of the total oxidation is much faster.

On the contrary, the noticeable catalytic enhancement observed for gold based monolith cannot be exclusively attributed to an additive effect from CO oxidation and WGS reactions. Indeed, the CO conversion obtained in the O_2-assisted WGS test exceeds by far the contribution of the direct CO oxidation (31%) in the whole temperature range. Consequently, this catalytic improvement can be clearly ascribed to an O_2-assisted WGS reaction. The capacity exhibited by the gold based catalyst (but not by the platinum based materials) to be assisted by oxygen species during the WGS reaction could be partially ascribed to the redox reaction pathway described for gold ceria catalysts. Although the role of ceria is clearly important no matter the NM (Pt or Au), it becomes absolutely necessary when gold is used as active phase due to its inability to dissociate water. The water dissociation is a slow step on the WGS reaction and, for gold based systems; it is

exclusively carried out by the support [23] or at the metal/support interface. In this sense, oxygen addition has been reported as a way to favor the water splitting due to the formation of active OH surface groups coming from the O_2 and H_2O reaction [35].

Besides this, the beneficial effect achieved by the oxygen addition could be also related to the inhibition of deactivation effects such as over-reduction of the support and/or formation of carbonaceous species over the catalytically active sites. Actually, it was reported that oxygen facilitates the carbonaceous intermediate species decomposition thus avoiding the active sites blockage during the WGS reaction [13].

On the other hand, a recent operando XAS study of Au/CeO_2 catalyst demonstrates that the optimum Ce oxidation state to carry out successfully the WGS is 3.3 [48]. Given the reductive atmosphere of the WGS, ceria over-reduction is likely to happen. However, the presence of oxygen traces could help to maintain cerium partially oxidized and close to the optimal formal valence to develop the WGS.

Overall, it appears that the beneficial effects depend on the noble metal nature, and oxygen seems to be consumed either by a parallel reaction, total CO oxidation for Pt, or by a support properties influence, reaction mechanism participation or optimal oxidation state maintenance in the case of gold based catalysts. In any case, our data reveal the successful application of the structured noble metal based catalysts in the O-assisted WGS, a fact that could represent a step forward in the process design.

4. Conclusions

An interesting comparison between structured gold and platinum noble metals supported on iron-doped ceria mixed oxide for WGS was carried out. The original powder catalysts were successfully deposited onto metallic monolithic structures achieving well fixed and homogeneous catalytic layer. Both monoliths and powders perform satisfactorily in the classical WGS, being Pt superior to Au in all cases. The scaling up from the powder to the structured catalysts seems to affect mainly to the gold based catalyst while the Pt monolith retains its excellent behavior, a fact not observed for the powder samples and reported here for the first time.

O_2 addition to the WGS feed stream changes the situation by boosting the WGS activity, greatly for Au and merely for Pt based monolith. Our data reveal that only the gold based monolith benefits for an actual "O_2 assisted WGS" reaction meanwhile the CO conversion increment observed for the Pt monolith results from the parallel CO oxidation reaction.

In any case, oxygen addition is a strategy to be considered to potentiate the WGS reaction over noble metals based structured catalysts especially for gold/ceria systems. Such an activity promotion together with the inherent features of the structured catalysts allowing smaller reactor volumes coverts our monoliths into an interesting alternative to be implemented in hydrogen fuel processors.

Acknowledgements

Financial support for this work has been obtained from Spanish Ministerio de Economía y Competitividad (MINECO) ENE2012-374301-C03-01 and ENE2013-47880-C3-2R and from Junta de Andalucía (TEP-8196) cofinanced by FEDER Funds from European Union. L. M. Martínez T. also acknowledge the Spanish "Ministerio de Ciencia e Innovación" for financial support (ref. no. JCI-2011-10059).

References

[1] C. Song, Catal. Today 77 (2002) 17-49.

[2] R.J. Farrauto, Y. Liu, W. Ruettinger, O. Ilinich, L. Shore, T. Giroux, Catal. Rev. 49 (2007) 141-196.

[3] C. Ratnasamy, J.P. Wagner, Catal. Rev. 51 (2009) 325-440.

[4] L.M. Martínez Tejada, M.I. Domínguez, O. Sanz, M. a. Centeno, J. a. Odriozola, Gold Bull. 46 (2013) 221-231.

[5] E. Tronconi, G. Groppi, Chem. Eng. Sci. 55 (2000) 6021-6036.

[6] P. Avila, M. Montes, E.E. Miró, Chem. Eng. J. 109 (2005) 11-36.

[7] V. Meille, Appl. Catal. A Gen. 315 (2006) 1-17.

[8] M. Flytzani-Stephanopoulos, B.C. Gates, Annu. Rev. Chem. Biomol. Eng. 3 (2012) 545-574.

[9] P. Liu, J.A. Rodriguez, J. Chem. Phys. 126 (2007) 164705-164710.

[10] G. Jacobs, S. Ricote, B.H. Davis, Appl. Catal. A Gen. 302 (2006) 14-21.

[11] G. Jacobs, E. Chenu, P.M. Patterson, L. Williams, D. Sparks, G. Thomas, B.H. Davis, Appl. Catal. A Gen. 258 (2004) 203-214.

[12] M. Gonzalez Castaño, T.R. Reina, S. Ivanova, M. a. Centeno, J. A. Odriozola, J. Catal. 314 (2014) 1-9.

[13] T.R. Reina, S. Ivanova, V. Idakiev, J.J. Delgado, I. Ivanov, T. Tabakova, M.A. Centeno, J.A. Odriozola, Catal. Sci. Technol. 3 (2013) 779-787.

[14] Y. Li, Q. Fu, M. Flytzani-Stephanopoulos, Appl. Catal. B Environ. 27 (2000) 179-191.

[15] O.H. Laguna, F. Romero Sarria, M. A. Centeno, J. A. Odriozola, J. Catal. 276 (2010) 360-370.

[16] A. Trovarelli, Catal. Rev. 38 (2006) 439-520.

[17] J. A. Rodriguez, S. Ma, P. Liu, J. Hrbek, J. Evans, M. Pérez, Science 318 (2007) 1757-1760.

[18] I.D. González, R.M. Navarro, W. Wen, N. Marinkovic, J. A. Rodriguez, F. Rosa, J.L.G. Fierro, Catal. Today 149 (2010) 372-379.

[19] W. Deng, M. Flytzani-Stephanopoulos Angew. Chem. Int. Ed. 2006, 45, 2285 –2289

[20] J. A. Rodriguez, J.C. Hanson, D. Stacchiola, S.D. Senanayake, Phys. Chem. Chem. Phys. 15 (2013) 12004-12025.

[21] G. Comelli, R. Rosei, Science 309 (2015) 752-755.

[22] T. Bunluesin, R.J. Gorte, G.W. Graham, Appl. Catal. B Environ. 15 (1998) 107-114.

[23] S. Seong, A.B. Anderson, J. Phys. Chem. 3654 (1996) 11744-11747.

[24] D. Çakír, O. Gülseren, J. Phys. Chem. C 116 (2012) 5735-5746.

[25] M. Haruta, Catal. Today 36 (1997) 153-166.

[26] W. Ruettinger, X. Liu, X. Xu, R.J. Farrauto, Top. Catal. 51 (2008) 60-67.

[27] A. Martinez-Arias, J.M. Coronado, R. Cataluna, J.C. Conesa, J. Soria, J. Phys. Chem. B 102 (1998) 4357-4365.

[28] Q. Fu, H. Saltsburg, M. Flytzani-Stephanopoulos, Science. 301 (2003) 935–938.

[29] X. Wang, R.J. Gorte, J.P. Wagner, J. Catal. 212 (2002) 225-230.

[30] C. Li, Y. Sakata, T. Arai, K. Domen, K. Maruya, T. Onishi, J. Chem. Soc. Faraday Trans. 1 85 (1989) 1451.

[31] J.M. Zalc, V. Sokolovskii, D.G. Löffler, J. Catal. 206 (2002) 169-171.

[32] A. Gayen, M. Boaro, C. De Leitenburg, J. Llorca, A. Trovarelli, J. Catal. 270 (2010) 285-298.

[33] X. Liu, W. Ruettinger, X. Xu, R. Farrauto, Appl. Catal. B Environ. 56 (2005) 69-75.

[34] N.K. Gamboa-Rosales, J.L. Ayastuy, M.P. González-Marcos, M. a. Gutiérrez-Ortiz, Catal. Today 176 (2011) 63-71.

[35] J. Kugai, J.T. Miller, N. Guo, C. Song, J. Catal. 277 (2011) 46-53.

[36] J. Barbier, D. Duprez, Appl. Catal. B Environ. 3 (1993) 61-83.

[37] V.G. Milt, S. Ivanova, O. Sanz, M.I. Domínguez, A. Corrales, J. A. Odriozola, M. A. Centeno, Appl. Surf. Sci. 270 (2013) 169-177.

[38] C. Rallan, A. Akah, P. Hill, A. Garforth, Indian Journal of Material Science 2013 (2013) Article ID 251495.

[39] D.M. Frías, S. Nousir, I. Barrio, M. Montes, L.M. Martínez T, M. A. Centeno, J. A. Odriozola, Appl. Catal. A Gen. 325 (2007) 205-212.

[40] S. Ivanova, C. Petit, V. Pitchon, Appl. Catal. A Gen. 267 (2004) 191-201.

[41] M.I. Domínguez, M. Sánchez, M.A. Centeno, M. Montes, J.A. Odriozola. Applied Catalysis A: General 302 (2006) 96–103.

[42] O.H. Laguna, M. González Castaño, M. A. Centeno, J. A. Odriozola, Chem. Eng. J. 275 (2015) 45-52.

[43] L.C. Almeida, O. Sanz, D. Merino, G. Arzamendi, L.M. Gandía, M. Montes, Catal. Today 215 (2013) 103-111.

[44] L. Pastor-Pérez, R. Buitrago-Sierra, A. Sepúlveda-Escribano, Int. J. Hydrogen Energ. 39 (2014) 17589-17599.

[45] F. Boccuzzi, A. Chiorino, M. Manzoli, D. Andreeva, T. Tabakova J.Catal 188 (1999) 176–185.

[46] T. R. Reina, S. Ivanova, M. A. Centeno, J. A.Odriozola Front. Chem. 2013; 1: 12.

[47] J.Z. Shyu, K. Otto, J. Catal. 115 (1989) 16-23.

[48] T.R. Reina, W. Xu, S. Ivanova, M.A. Centeno, J. Hanson, J. A. Rodriguez, J.A. Odriozola, Catal. Today 205 (2013) 41-48.

Figure Captions

Figure 1: XRD patterns of the prepared solids.

Figure 2: SEM microphotographs of the M_Au/CeFe catalyst: A) front; B) cross section view.

Figure 3: H_2-TPR profiles of the prepared catalysts and the ceria-iron support.

Figure 4: Catalytic activities of Pt_CeFe, Au_CeFe, S_Pt/CeFe and S_Au/CeFe samples in classical WGS mixture at $4000h^{-1}$.

Figure 5: CO conversions of M_Pt/CeFe and M_Au_CeFe catalysts: A) CO conversions at GHSV = 4000 h^{-1} in classical WGS reaction (4.5% CO + 30% H_2O) and "O_2-assisted" conditions (4.5% CO + 30% H_2O + 0.7% O_2); B) CO conversions at GHSV = 4000 h^{-1} in CO oxidation reaction (4.5% CO + 0.7% O_2).

Table 1. Chemical composition and textural properties of the synthetized solids.

	Al_2O_3 (wt. %)	CeO_2 (wt. %)	Pt or Au (wt. %)	Fe_2O_3 (wt. %)	S_{Bet} (m^2/g)	V_{Pore} (cm^3/g)
Al_2O_3	100	-	-	-	202	0.36
CeFe	84.1	14.4	-	1.5	172	0.38
Au/CeFe	82.4	13.6	2.6	1.4	182	0.40
S_Au/CeFe	84.2	12.2	2.3	1.2	185	0.41
Pt/CeFe	76.1	19.3	2.3	2.2	175	0.38
S_Pt/CeFe	78.1	17.7	2.2	2	181	0.40

Figure 1

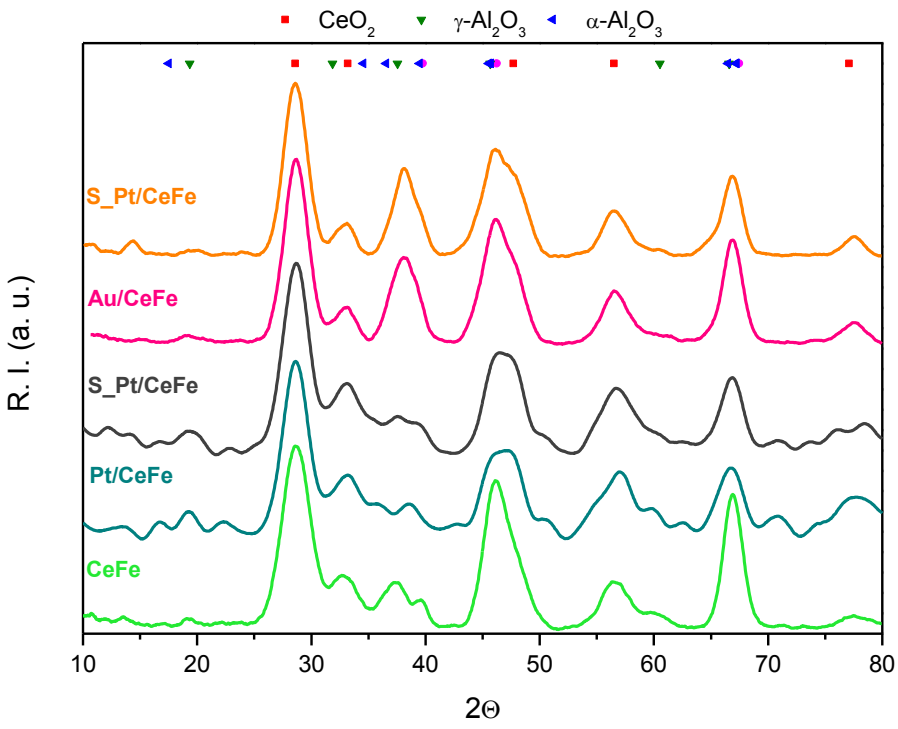
CeO2
γ-Al2O3
α-Al2O3
S_Pt/CeFe
Au/CeFe
S_Pt/CeFe
Pt/CeFe
CeFe
R. I. (a. u.)
10
20
30
40
50
60
70
80
2Θ

Figure 2

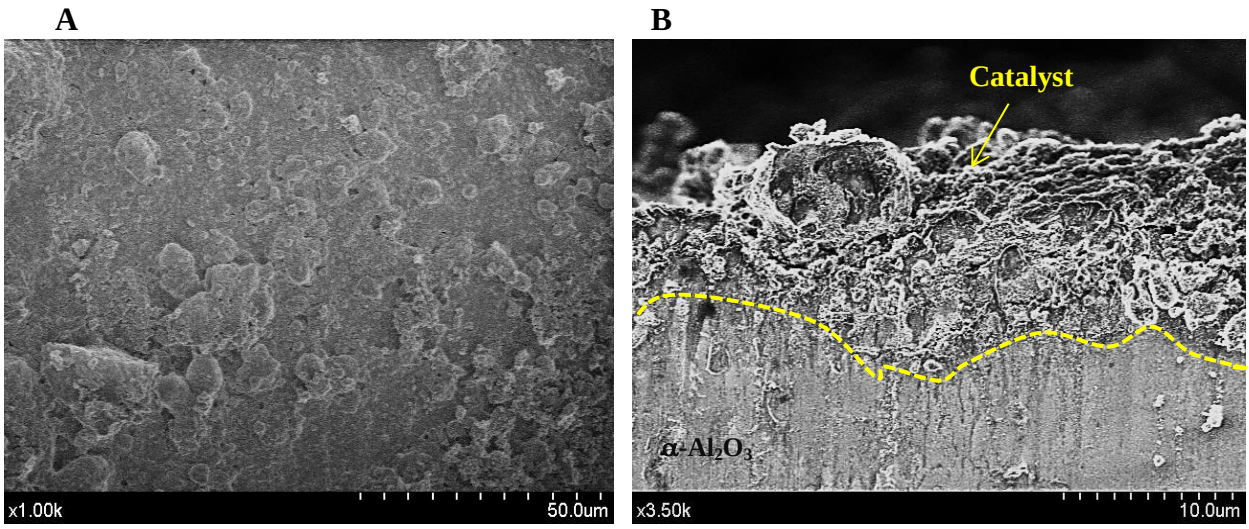

Figure 3

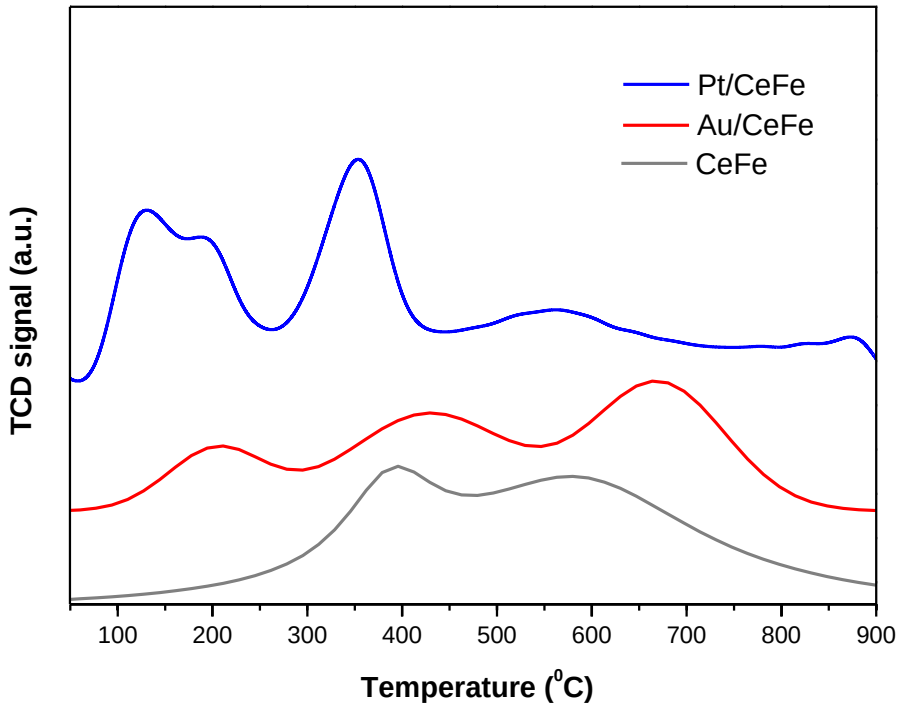
Pt/CeFe
Au/CeFe
CeFe
TCD signal (a.u.)
100
200
300
400
500
600
700
800
900
Temperature (0C)

Figure 4

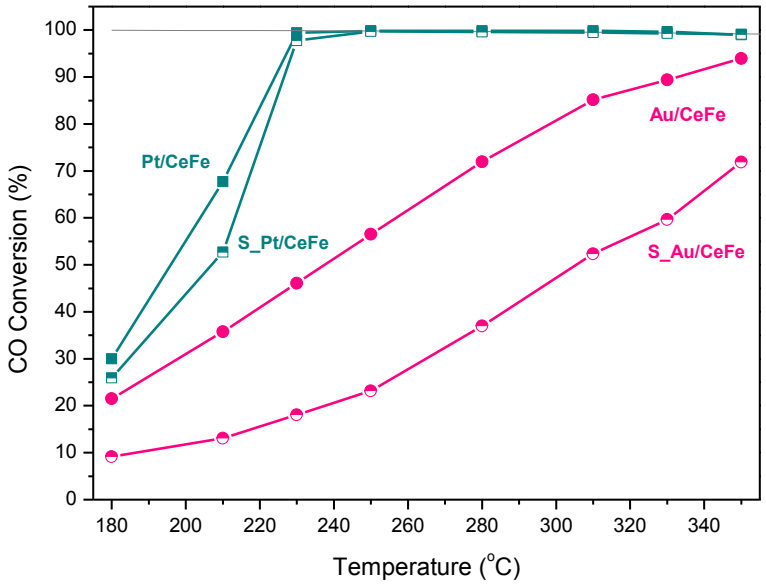
CO Conversion (%)
Temperature (°C)
Pt/CeFe
S_Pt/CeFe
Au/CeFe
S_Au/CeFe
0
10
20
30
40
50
60
70
80
90
100
180
200
220
240
260
280
300
320
340

Figure 5

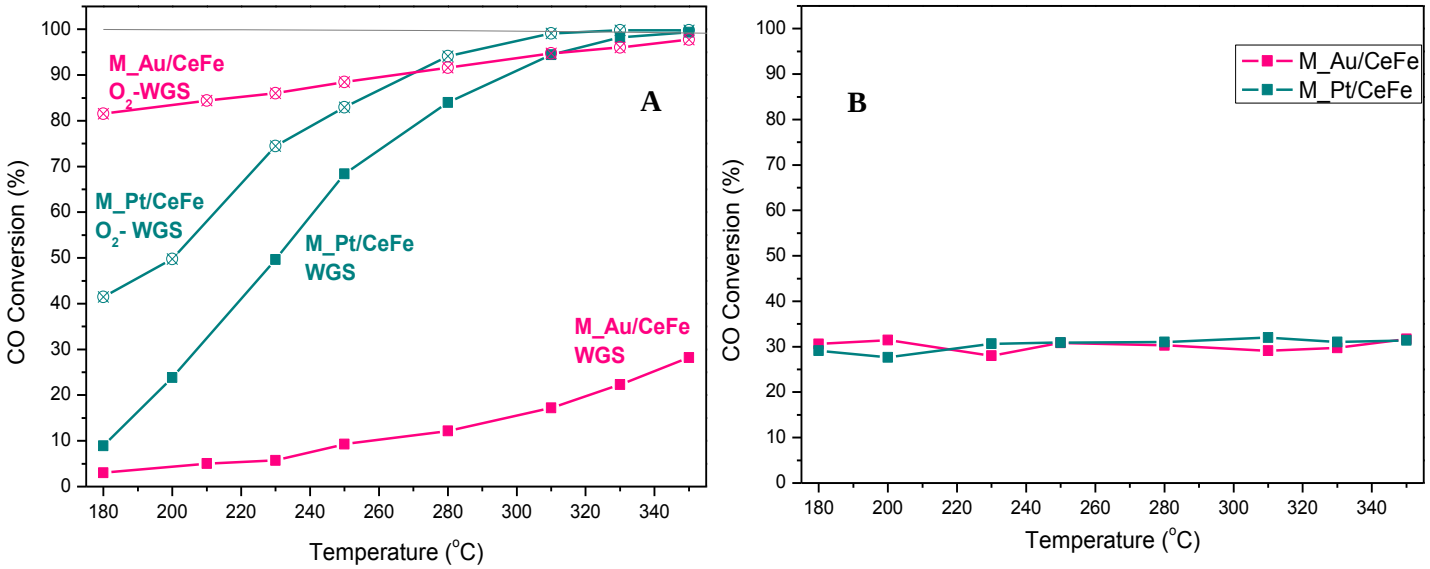
CO Conversion (%)
Temperature (°C)
M_Au/CeFe
O2-WGS
M_Pt/CeFe
O2- WGS
M_Pt/CeFe
WGS
M_Au/CeFe
WGS
A
B
M_Au/CeFe
M_Pt/CeFe